Failure issues of brick masonry

B. Blackard, B. Kim, C. Citto, K. Willam & S. Mettupalayam
CEAE Department, University of Colorado-Boulder, Boulder, Colorado

ABSTRACT: This paper focuses on the fundamental meso-mechanical failure processes in masonry prisms when composite clay bricks bonded by cement mortar are subjected to axial compression. There are several intriguing issues which complicate the failure of the masonry composite because of the subtle interaction effects between the clay brick units and the weaker cement mortar. In fact, 3-D analysis is required to fully penetrate the failure mode which is governed by biaxial tension-compression of the solid brick rather than triaxial compression of the mortar. Dimensional reduction in the form of 2-D plane stress analysis leads to erroneous mode conversion and to significant underestimation of the compression capacity of the masonry prism which depends primarily on the tensile strength of the brick unit. In other terms, the out-of-plane confinement plays a critical role in the assessment of the overall compression capacity of masonry walls.

1 INTRODUCTION

Due to the composite construction of masonry, progressive failure is a complicated process. Masonry consists of two components, brick units and mortar joints which exhibit very different stiffness and strength properties. Moreover, both constituents have a low tensile strength when compared to their compressive counterparts. Consequently, a masonry wall in compression does not necessarily fail in compression of the weakest component but can fail in tension due to mismatch conditions in the composite. Aside from the large strength variations of the two components it is the bond among the brick unit and the mortar which determines the critical failure path in a masonry wall.

The current computational-experimental study focuses on the critical failure mode and the question whether three dimensional analysis is required to capture in-plane as well as out-of-plane failure modes or whether two dimensional failure simulations do suffice. To this end continuum based finite elements are employed for meso-modeling of the brick and mortar response of a masonry prism subjected to compression. The test article consists of five solid clay brick units which are mortared by four layers of cement mortar. The nonlinear failure simulations resort to the damage-plasticity model by Lee and Fenves [1998] which has been incorporated into Abaqus [Version 6.5]. Appropriate material tests on brick units and cement mortar were carried out in-house in conjunction with the current NEESR-SG research project [Seismic Performance Assessment and Retrofit of Non-Ductile RC Frames with Infill Walls]. Thereby the main objective is to validate the computational results with the experimental data of masonry prisms.

2 MATERIAL MISMATCH

A key issue in the failure mechanism of a masonry prism is the initial mismatch of the elastic properties of brick and mortar. Assuming isotropy the elastic moduli E^m , E^b in concert with the Poisson numbers ν^m , ν^b govern the cross-effect of axial compression in the form of the in-plane and out-of-plane lateral strain. If the interfaces between the mortar and brick were allowed to slip freely, the two material components would deform laterally by differing amounts except for a special condition which is detailed below. The result of this mismatch of lateral deformation is that friction restrains and hence compresses the mortar joints from free lateral expansion because of the stiffer brick units, which in turn experience lateral tension. This can be readily explained from examining the compliance relationships of isotropic linear elastic materials and their interaction along bimaterial interfaces.

Considering the masonry prism in Figure 2 where the y-axis refers to the direction of axial compression and the x- and z- coordinates the lateral direc-

tions. The normal strains in the x-direction of the brick unit and the cement mortar are according to generalized Hooke's law,

$$\varepsilon_x{}^b = \frac{1}{E^b}\left[\sigma_x - \nu\sigma_y - \nu\sigma_z\right]^b$$
$$\varepsilon_x{}^m = \frac{1}{E^m}\left[\sigma_x - \nu\sigma_y - \nu\sigma_z\right]^m \qquad (1)$$

Under axial compression equilibrium dictates that $\sigma_y{}^b = \sigma_y{}^m = \sigma_y$. Assuming for the time being that the lateral stresses remain zero because of no frictional restraint then the lateral strains are directly proportional to the compliance relations,

$$\varepsilon_x{}^b = -\frac{\nu^b}{E^b}\sigma_y \;; \quad \varepsilon_x{}^m = -\frac{\nu^m}{E^m}\sigma_y \qquad (2)$$

In other terms the lateral compliance is directly proportional to the ratio $c_{lat} = \nu/E$. In contrast under full bond and adherence of the two components at the bimaterial interface strong compatibility requires that the lateral strains in the brick and mortar in Equation (1) are equal. Assuming $\sigma_x{}^m = \sigma_z{}^m$ and $\sigma_x{}^b = \sigma_z{}^b$ this leads to the critical condition of no lateral mismatch under axial stress σ_y when,

$$\nu^b E^m = \nu^m E^b \quad \text{or} \quad n = \frac{c_{\text{lat}}{}^m}{c_{\text{lat}}{}^b} = 1 \qquad (3)$$

In other terms, if the ratio of the lateral compliances $n = 1$, then there is no mismatch between the lateral deformations of the two materials.

Using equilibrium the lateral stresses in the brick and mortar components may be related to each other by a statement of self-equilibrium, $\sigma_x{}^m = -r\sigma_x{}^b$ and $\sigma_z{}^m = -r\sigma_z{}^b$ where $r = t^b/t^m$ denotes the thickness ratio of the brick unit over the mortar joint. This condition has been introduced by Berto et al. [2005] in order to develop the explicit expressions below for the lateral stresses in the brick unit and the mortar joint in terms of the axial stress σ_y,

$$\sigma_x{}^b = \sigma_z{}^b = \frac{\nu^b E^m - \nu^m E^b}{E^m + \frac{t^b}{t^m}E^b - E^m\nu^b - \frac{t^b}{t^m}E^b\nu^m}\sigma_y$$
$$\sigma_x{}^m = -\frac{t^b}{t^m}\sigma_x{}^b \quad \text{and} \quad \sigma_z{}^m = -\frac{t^b}{t^m}\sigma_z{}^b \qquad (4)$$

The assumptions for this expression are as follows:

1. The vertical stress is uniform throughout both components of the prism
2. There is no slip along the brick/mortar interface
3. There is a state of uniform lateral stress within each material
4. There is no stress transfer through interface shear

It is the differential equilibrium condition which restricts the validity of the two expressions in Equation (4) to the two axial planes of symmetry in the center of the masonry prism. Clearly at the surface of the prism all lateral tractions must vanish. Therefore large shear stresses must develop near the lateral faces of the prism (a) in order to diminish the mismatch of the lateral normal stresses and (b) to reduce the magnitude of the surface tractions to zero ($\sigma_x{}^b = \sigma_x{}^m = 0$ at the lateral x-faces and $\sigma_z{}^b = \sigma_z{}^m = 0$ at the free lateral z-faces).

In Equation (4) σ_y is negative for the case of a prism loaded in axial compression. It can be easily verified from Equation (4) that the lateral normal stresses are zero when the mismatch condition $n = 1$. It is also elementary to recognize that the lateral brick stresses are positive in tension, $\sigma_x{}^b = \sigma_z{}^b > 0$, when $n > 1$, while the lateral mortar stresses are in compression, $\sigma_x{}^m = \sigma_z{}^m < 0$. Together with the axial compression $\sigma_y < 0$ this leads to a fracture critical state of equibiaxial tension-compression in the brick and to a forgiving state of triaxial compression in the mortar. Note the opposite result occurs for $n < 1$ when the brick unit is laterally more compliant than the mortar, resulting in a fracture critical state of equibiaxial tension-compression in the mortar rather than in the brick.

An extension of these results can be obtained by considering a transversely anisotropic brick model. Assuming the extrusion direction (vertical prism direction) of the brick to be the principal axis of transverse anisotropy, the axial brick stiffness differs from the lateral one. In this case three additional elastic material properties are needed, $E_y{}^b$, $\nu_{yx}{}^b = \nu_{yz}{}^b$, $G_{yx}{}^b = G_{yz}{}^b$ beyond the two isotropic moduli in the plane of the brick unit, $E_{xz}{}^b$ and $\nu_{xz}{}^b$:

$E_y{}^b$ = brick modulus of elasticity in axial y-direction
$E_{xz}{}^b$ = brick modulus of elasticity in the lateral x, z-directions (isotropic x-z plane)
$\nu_{yx}{}^b = \nu_{yz}{}^b$ = brick Poisson ratio relating the axial and any lateral x-, z-direction
$\nu_{xz}{}^b$ = brick Poisson ratio relating the two lateral x-z directions (isotropic x-z plane)
$G_{yx}{}^b = G_{yz}{}^b$ = brick shear modulus relating axial and lateral directions
E^m = [isotropic] mortar modulus of elasticity
ν^m = [isotropic] mortar Poisson ratio

Starting from the transversely anisotropic elastic compliance equations for brick and mortar:

$$\varepsilon_x{}^b = \frac{1}{E_{xz}{}^b}\sigma_x{}^b - \frac{v_{yx}{}^b}{E_y{}^b}\sigma_y{}^b - \frac{v_{xz}{}^b}{E_{xz}{}^b}\sigma_z{}^b$$

$$\varepsilon_z{}^b = -\frac{v_{xz}{}^b}{E_{xz}{}^b}\sigma_x{}^b - \frac{v_{yx}{}^b}{E_y{}^b}\sigma_y{}^b + \frac{1}{E_{xz}{}^b}\sigma_z{}^b \qquad (5)$$

$$\varepsilon_x{}^m = \frac{1}{E^m}\sigma_x{}^m - \frac{v^m}{E^m}\sigma_y{}^m - \frac{v^m}{E^m}\sigma_z{}^m$$

$$\varepsilon_z{}^m = -\frac{v^m}{E^m}\sigma_x{}^m - \frac{v^m}{E^m}\sigma_y{}^m + \frac{1}{E^m}\sigma_z{}^m$$

and making the same assumptions as with the isotropic model, the lateral normal stresses in the brick units and mortar joints turn out to be:

$$\sigma_z{}^b = \sigma_x{}^b = \frac{E_{xz}^b}{E_y^b}\frac{\mathrm{A}+\mathrm{B}}{\mathrm{C}^2-\mathrm{D}^2}\sigma_y$$

$$\sigma_z^m = \sigma_x^m = -r\sigma_x^b$$

where (6)

$$\mathrm{A} = \left(E^m v_{yx}{}^b - E_y{}^b v^m\right)\left(E^m + E_{xz}{}^b r\right)$$

$$\mathrm{B} = \left(E^m v_{yx}{}^b - E_y{}^b v^m\right)\left(E^m v_{xz}{}^b + E_{xz}{}^b v^m r\right)$$

$$\mathrm{C} = E^m + E_{xz}{}^b r$$

$$\mathrm{D} = E^m v_{xz}{}^b + E_{xz}{}^b v^m r$$

Although this complicates direct interpretation of the cross effect between axial compression and lateral expansion/stresses the condition for zero mismatch leads to the same condition $n = 1$ in analogy to Equation (3) whereby $c_{lat}{}^b = v_{yx}{}^b / E_y{}^b$. Also note that the shear stiffness properties do not appear in these expressions because the principal stress coordinates are assumed to coincide with the principal axes of transverse anisotropy, and because only normal components are considered in the derivation of Equation (6).

3 EXPERIMENTAL RESULTS

Bricks, mortar, and masonry prisms were tested at the University of Colorado structural materials laboratory. Table 1 displays the average results of these experiments indicating reasonable correlation with COV values varying between 3-15%. So far a total of 9 bricks, 4 mortar cylinders, and 5 prisms were tested in axial compression and tension. The bricks had dimensions 4.5"×3.75"×2.25" and the mortar joints were 0.375" thick. The mortar mix consisted of a sand:cement:lime ratio of 5:1:1. The normalized axial response behavior of the five prism experiments are shown in Figure 1 together with that of brick and mortar. Note that complete stress-strain data was collected for only two brick specimens.

The brick tests were performed after capping the clay units with a thin layer of gypsum capping compound. The bricks were stored under ambient conditions. The compression tests on the cement mortar were performed on 4"x8" cylinders which were cured 28 days in the fog room before capping and testing. The prisms were covered with plastic and cured for 28 days under ambient conditions before testing. The construction of the prisms included wetting each brick for approximately 10 seconds before placement. The test data are summarized in Table 1 and shown in Figure 1.

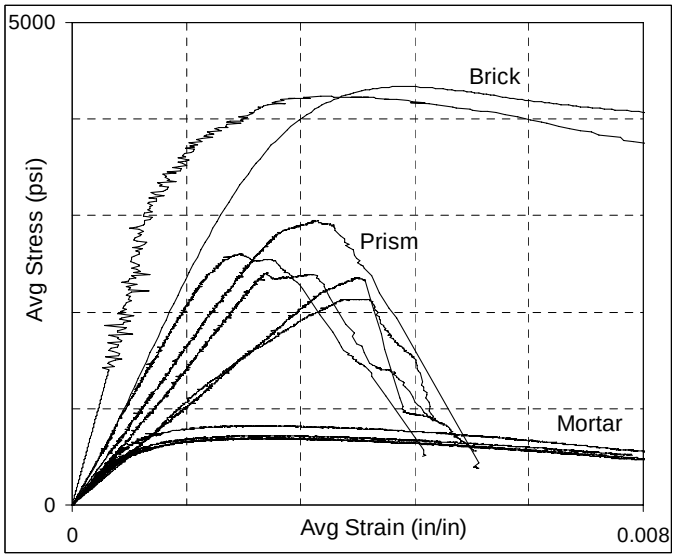

Figure 1. Experimental data from prism, brick and mortar tests.

Table 1. Average material properties from testing

	Brick	Mortar	Prism
Comp. Strength (psi) [COV]	4,840 [15.2%]	732 [8.4%]	2,490 [9.8%]
Tensile Splitting Strength (psi) [COV]	372 [12.5%]	141 [3.2%]	------
Modulus of Rupture (psi) [COV]	640 [8.6%]	------	------

4 3D NUMERICAL SIMULATIONS

A three dimensional finite element prism model was created with 4653 nodes and 3600 first order hexahedra elements resulting in 13959 DOF. The commercial software Abaqus Version 6.5 was used for the finite element analyses. Figure 2 illustrates the 3D model, and Figure 3 shows the deformed mesh along with the equivalent plastic strain. Figure 3 clearly shows the lateral "bursting" in the middle brick which is the dominant failure mechanism in the masonry prism.

The material properties used for the numerical analyses are listed in Table 2. The damage plasticity concrete formulation by Lee & Fenves [1998] was used for both materials. The parameters K, f_{bo}/f_{co} and ecc determine the initial shape of the failure surface, where K defines the out-of roundness of the deviatoric trace, the strength ratio f_{bo}/f_{co} the increase of equibiaxial compression over uniaxial compression and hence the internal friction, and ecc the rounding factor of the equitriaxial tensile vertex on the hydrostat. The dilation angle Ψ specifies the direction of the (non-associated) plastic flow. The tensile fracture energy describes the initial energy release after the peak stress is reached in tension. Tensile exponential decay was specified with the fracture energy shown in Table 2. There was no damage considered in the brick and mortar elements in order to simplify the constitutive input of the damage-plasticity model in Abaqus.

Table 2. Material properties (damage plasticity)

	Brick	Mortar
Modulus of Elasticity (psi)	3.0×10^6	5.0×10^5
Poisson ratio	0.1	0.2
Uniaxial Comp. Strength (psi)	4,840	732
Uniaxial Tensile Strength (psi)	372	141
Tensile Fracture Energy G_I(lb/in)	0.46	0.34
Dilatancy Angle Ψ	20°	20°
Friction Angle	19°	19°
Deviatoric Out-of- Roundness K	0.7	0.7
Biaxial Strength Ratio f_{bo}/f_{co}	1.15	1.15
Vertex Rounding ecc	0.1	0.1

The 3D model was analyzed with and without lateral restraints at the top and bottom faces of the prism. Figure 4 illustrates the average stress-strain response of both the constrained and unconstrained 3D prism models. Very little difference is evident in the two results. This may be due to the localized effect of the top and bottom boundary conditions. With the prisms under consideration having an aspect ratio of 3.4, these end effects become insignificant. Figure 4 also includes the input data of the compression calibration curves for the mortar and brick. As expected, the prism behavior falls between the mortar and brick response in axial compression.

Figure 5 shows the shear stress contours in the x-y plane at a center mortar joint immediately before plastic behavior began in the prism. The mortar is clearly being restrained from lateral expansion by the surrounding brick material due to interface shearing, which causes the brick to be in a state of bilateral tension-compression.

A comparison of the 3D numerical model and the analytical approximation in Equation (4) is displayed in Figure 6. The brick stresses were taken at the center of the middle brick, and the mortar stresses at the center of the adjacent mortar joint. Clearly the stresses in the mortar agree very well up to the peak prism stress. The stresses in the brick agree well at low stress levels, but start to diverge from the analytical solution before the peak prism stress is reached. This can be explained by the nature of the analytical approximation. Equation (4) represents the entire cross effect of axial compression in terms of two values, one for the mortar and one for the brick. This is a good approximation for the thin mortar layer, but it is a poor approximation for the much thicker brick with a large stress variation.

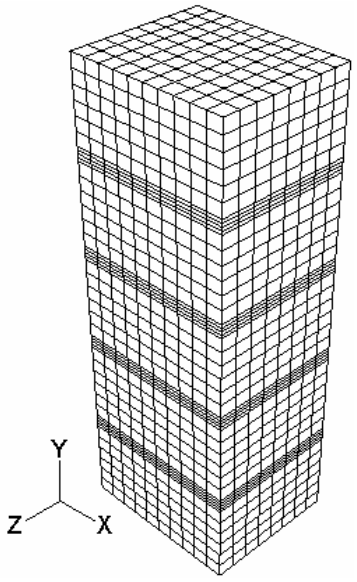

Figure 2: 3D finite element mesh

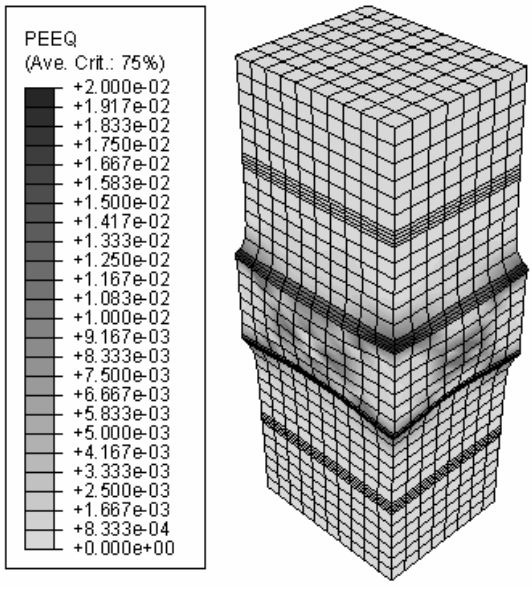

Figure 3. Deformed shape and equivalent plastic strain (deformation scale = 20).

It is interesting to note that in the finite element model, the lateral stresses in the brick are no longer the same in the x- and z-directions as contrast to the analytical solution. An explanation for this emerges from the simplifying assumptions leading to Equation (4) in which the different geometry in the lateral directions of the prism is neglected. In reality the different lateral dimensions of the prism result in different response behavior in the x- and z-directions, as seen in the finite element results of the brick response which turns very pronounced close to failure.

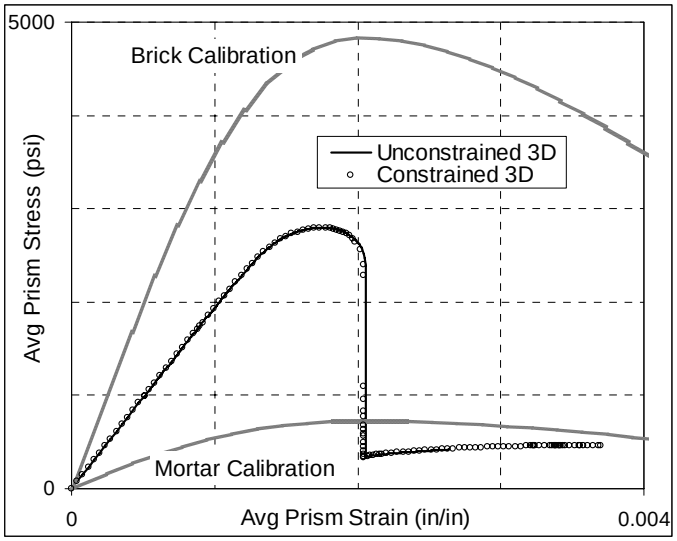

Figure 4. 3D model prism response.

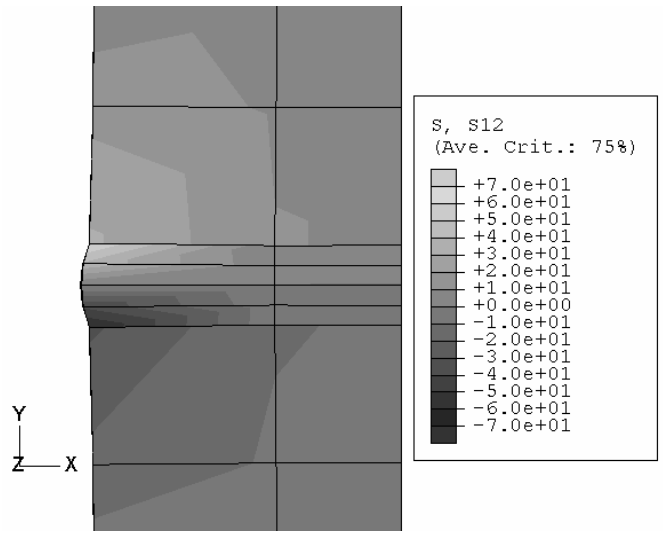

Figure 5. Shear stresses at mortar joint (Deformation Magnification = 500).

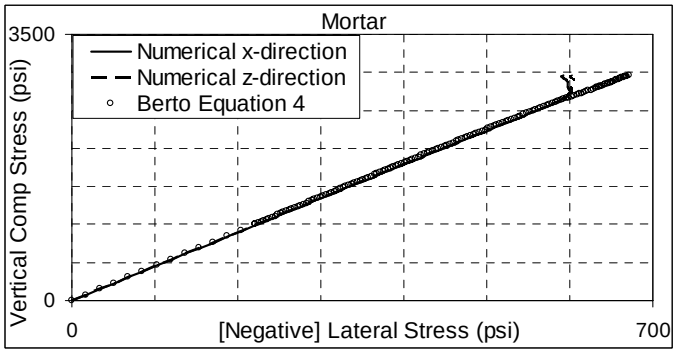

Figure 6A. A comparison of the numerical and analytical results (center of prism).

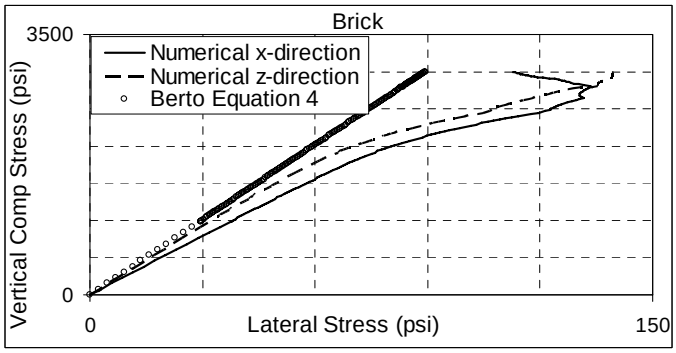

Figure 6B. A comparison of the numerical and analytical results (center of prism).

5 MESH SENSITIVITY

The "standard" 3D mesh consists of brick units that are 6 elements high, 10 elements wide, and 8 elements deep, as can be seen in figure 2. The mortar joints have 4 layers of solid elements through their thickness. In addition three coarser meshes were considered. The first, "coarse mesh 2", implements bricks of 3 elements high, 6 elements wide, and 4 elements deep, while 2 element layers comprise the thickness of the mortar joint. The second, "coarse mesh 1" uses the same mesh as "coarse mesh 2", except that the mortar joints are comprised of only 1 element layer through their thickness. The third, "coarse mesh 0" is the same as "coarse mesh 1", except cohesive interface elements replace the single layer of mortar elements. All 3D solid elements are trilinear 8 node hexahedral elements using full integration. The average stress-strain results for these three models are shown in Figure 7. The finite element models show close agreement with respect to mesh refinement in spite of the large drop of axial load resistance shortly after peak. Of particular interest are the nearly identical results for the single and double element layers used to idealize the mortar joint. This is due to the tension in the brick being the dominant source of prism failure. In contrast, the model using a single layer of cohesive interface elements for the mortar joint (designated as "coarse mesh 0") does result in a failure mechanism which is totally different from that of a single layer of finite thickness continuum elements. In fact, the zero-thickness cohesive interface element does not cap-

ture the lateral mismatch between brick and mortar and simply reproduces the brick calibration curve in compression as shown in Figure 4. In other terms the cohesive interface model in Abaqus [Version 6.5] does not activate damage in compression and hence the masonry prism behaves like a single brick mainly because of the missing normal stress and strain components tangential to the interface, see e.g. Willam, Rhee & Shing [2004].

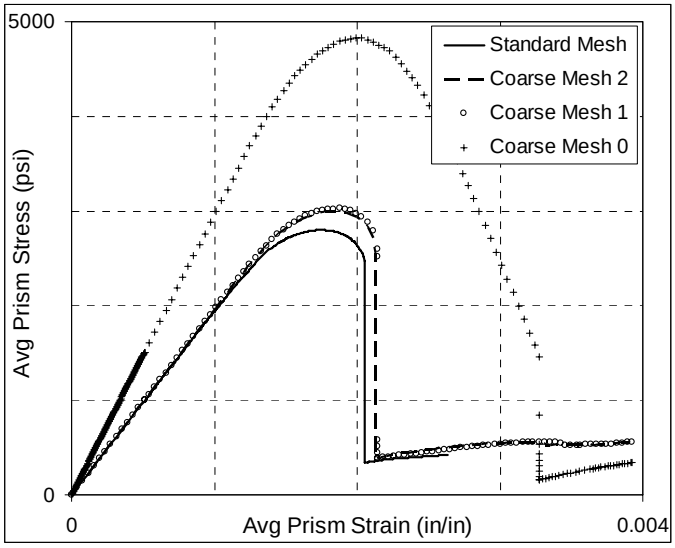

Figure 7. Mesh sensitivity study.

6 THREE PLANAR MODELS

For meso-studies of full-scale masonry structures detailed 3D finite element models are still prohibitive in cost. Consequently 2D failure simulation models need to be assessed whether they are capable of reproducing the governing failure mechanism in the composite masonry prism, see e.g. Anthoine [1997]. Assuming plane stress, plane strain and generalized plane strain options all dimensional reductions are based on the standard mesh with 517 nodes and 460 elements, resulting in 1551 DOF, as illustrated in Figure 8. This leads to a large reduction of DOF by nearly tenfold and an even greater saving of computational resources because of the narrow bandwidth. The same damage-plasticity model is used for the material description as in the 3D analysis. The boundary conditions are laterally unconstrained at the top and bottom platen/specimen interfaces as before. The generalized plane strain option in Abaqus is based on the 3D formulation in which the out-of-plane motion is confined by two rigid bounding planes whose relative separation is controlled by a reference node implementing out-of-plane DOF 3. The in-plane DOF in the two bounding planes are subject to equality constraints eliminating the out-of-plane shear deformations but accounting for the out-of-plane normal strain. This is consistent with the observations by Li & Lim [2005] where a mixed variational formulation has been developed to capture generalized plane strain in terms of an additional DOF.

As can be seen from figure 9, the plane strain and generalized plane strain models show a higher peak stress than the 3D model. The plane strain model reproduces the brittle in-plane failure mode present in the 3D model. The generalized plane strain model peaks closer to the 3D results than the plane strain model. However the very brittle post-peak behavior of the 3D mesh is reduced in favor of a more ductile response. The plane stress model shows dismal results, diverging from the linear elastic range far too early, and then failing to converge soon after. This premature failure is due to the change of the underlying failure mechanism from biaxial tension-compression in the brick units to biaxial compression in the mortar joints due to the lack of out-of-plane confinement. In short, the two dimensional reduction of the stress state introduces a dramatic change of the failure mode. Similarly to the 3D simulations the plane strain model provides lateral confinement in both components, in fact it prohibits out-of-plane failure in both brick and mortar, and henceforth leads to an upper bound. The generalized plane strain analysis provides an intermediate solution, the out-of-plane movement reduces the amount of plane confinement in the brick and in the mortar. For this reason, the generalized plane strain model is being used for the computationally intense parameter studies in the remainder of the paper.

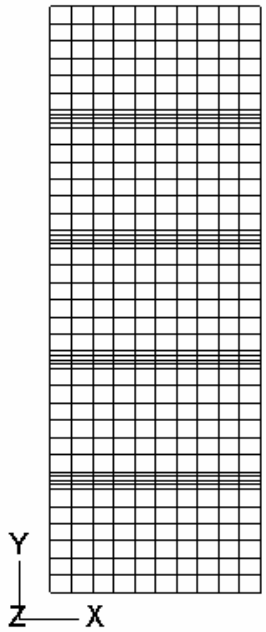

Figure 8: Finite element mesh for the planar models.

7 THE EFFECT OF BRICK TENSILE STRENGTH

With the biaxial tension-compression state of brick stress being considered to be the critical failure mechanism, one would expect that the brick tensile strength plays the dominant role in the overall strength of the masonry prism. For this reason the generalized plane strain model was used to study the effect of the tensile brick strength which was varied from f_t^b =100 psi to f_t^b =1000 psi, leaving all of the other parameters unchanged.

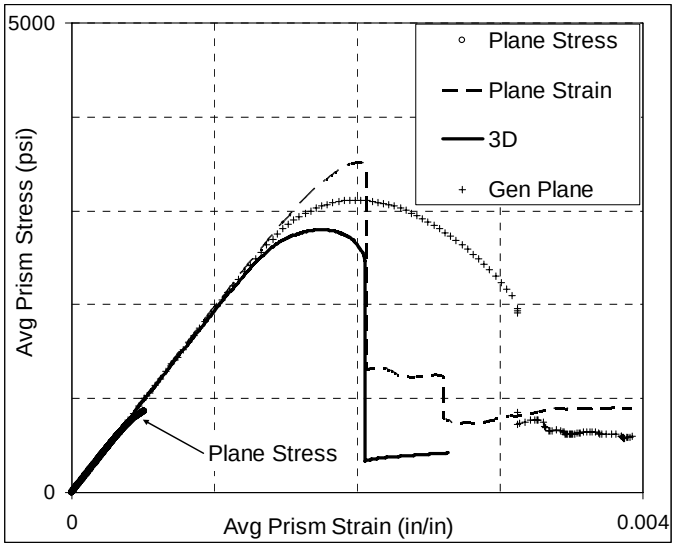

Figure 9. A comparison of the four FEM models.

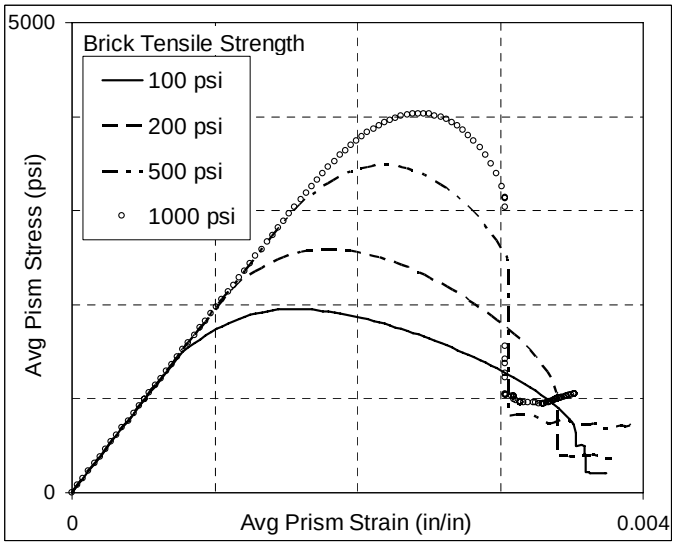

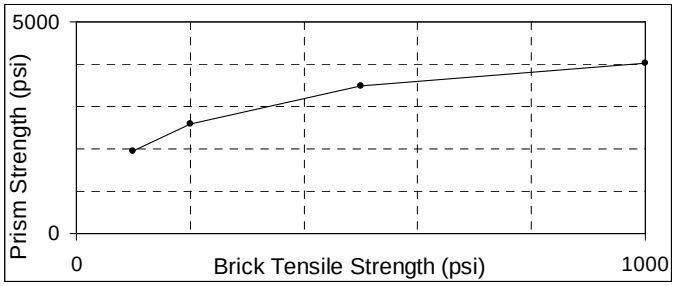

Figure 10. The effect of brick tensile strength on the prism compression strength.

Figure 10 shows the results of this study. As expected, the increase in the brick tensile strength increases the compressive capacity of the prism by over 100%. The fact that the prism strength gradually approaches the axial compression capacity of the brick unit supports the observation that prism failure develops first in biaxial tension-compression in the brick for which the axial compression strength provides an upper bound.

8 THE EFFECT OF MORTAR JOINT PROPERTIES

In terms of composite analysis one would expect that the amount of mortar should play some role in the stiffness and strength properties of the prism. To this end the thickness of the mortar joint was varied from 0.1" to 0.375". The expectation is that a thicker mortar joint would reduce the stiffness of the prism. Because of the compliance mismatch in Equation (4) a higher tensile stress should develop in the brick and as a result the prism would fail at a lower compression stress. The results are displayed in Figure 11. As can be seen, decreasing the thickness of the mortar joint increases the stiffness of the prism and its compressive strength by over 30%.

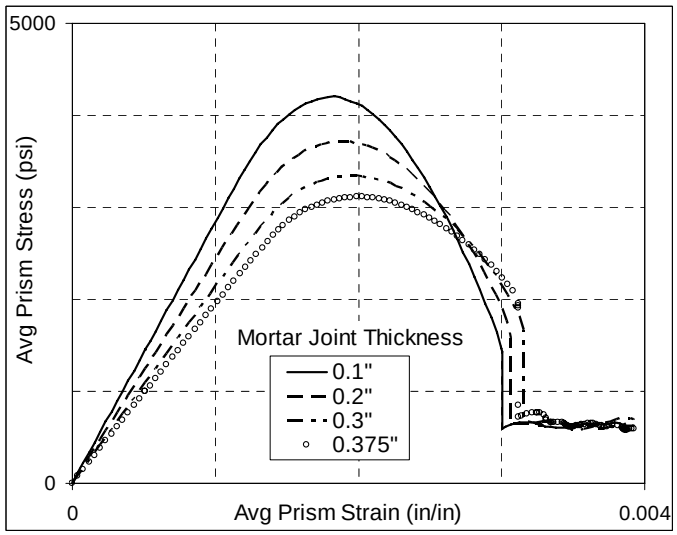

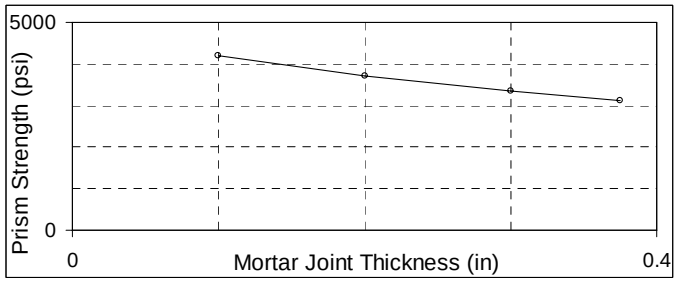

Figure 11. The effect of mortar joint thickness on the prism compression strength.

In contrast Figure 12 illustrates the comparatively small effect of the mortar capacity on the prism strength which increases by less than 15% if one triples the mortar compression strength. As one would

expect, a stronger mortar means a stronger prism. However, the mortar strength plays little role in the failure mechanism of the masonry prism which is governed by biaxial tension-compression in the brick unit rather than by triaxial compression in the mortar. However all failure simulations indicate that there is a residual strength of the prism after the large drop of load capacity has taken place which at first appears to be related to the compression strength of the mortar. However considering its invariance in Figure 12 it appears that both the peak as well as the residual value of compressive prism strength are closely related to the tensile capacity of the brick as shown in Figure 10.

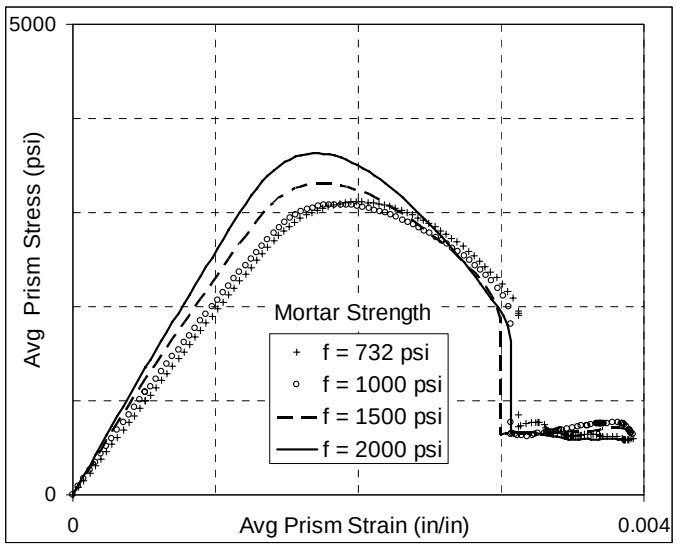

Figure 12: The effect of mortar compression strength on the prism compression strength.

9 SUMMARY OF PRISM STRENGTH

Table 3 compares the axial strength results of the 2D and 3D finite element models with the prism test data. The 3D model furnishes a prism strength which agrees well with the experimental result, it is 12% higher than the average of the experimental prism data with a COV of 9.8%. The plane strain peaks 41% higher, while the generalized plane strain peaks 25% higher. Due to the erroneous failure mode, the plane stress result yields a prism strength which is 65% lower than the test data.

Table 3. A comparison with test results

	Prism Strength
Experimental	2,490 psi
3D FE-Model	2,797 psi
Plane Strain	3,514 psi
Generalized Plane Strain	3,113 psi
Plane Stress	860 psi

The discrepancy among the test data and the numerical results may be in part due to the lack of test data to calibrate the large number of material parameters of the damage-plasticity model in Abaqus. In view of the experimental variations and the uncertainties in all input parameters the 3D model provides fairly close agreement, although the generalized plane strain model may be an acceptable alternative to capture the main features of masonry and to reduce computational effort.

10 CONCLUSIONS

The present computational and experimental studies illustrate the failure mechanism of a masonry prism in compression. For a better understanding of the failure processes the effect of several material and geometric properties were investigated with the aid of 2D and 3D finite element models. The results demonstrate that full 3D simulations are warranted when the proper failure mechanism is to be captured. The parameter studies indicate that the tensile strength of the brick has a significant effect on the prism strength which is far greater than the effect of the mortar properties. In fact the thickness of the mortar joint is much more significant than the compression strength of the mortar.

ACKNOWLEDGEMENTS

The authors wish to acknowledge the support of this research effort by the US National Science Foundation under NSF NEESR-SG award no. 0530709. The close collaboration and exchange with Prof. Benson Shing at UCSD and Prof. Sarah Billington at Stanford University are much appreciated on the joint project “Seismic Performance Assessment and Retrofit of Non-Ductile RC Frames with Infill Walls”. Opinions expressed in this paper are those of the authors and do not necessarily reflect those of the sponsor.

REFERENCES

ABAQUS, inc., Abaqus version 6.5 finite element software, 2004, Providence RI, USA

Anthoine, A.1997. Homogenization of Periodic Masonry: Plane Stress, Generalized Plane Strain or 3D Modelling?, Communications in Numerical Methods in Engineering 13: 319-326.

Berto, L., Saetta, A., Scotta, R., Vitaliani, R. 2005. Failure Mechanism of Masonry Prism Loaded in Axial Compression: Computational Aspects, Materials and Structures, 38: 249-256.

Lee, J., Fenves, G. 1998. A Plastic-Damage Concrete Model for Earthquake Analysis of Dams, Earthquake Engineering and Structural Dynamics, 27: 937-956.

Li, S., Lim, S. 2005. Variational Principles for Generalized Plane Strain Problems and their Applications, Composites: Part A, 36/3: 353-365.

Willam, K., Rhee, I., Shing, B. 2004. Interface Damage Model for Thermomechanical Degradation of Heterogeneous Ma-

terials, Computer Methods in Applied Mechanics and Engineering, 193: 3327-3350.